Images of Photoelectrons Formed in Intense Laser Fields

H. Helm, N. Bjerre, M. J. Dyer, D. L. Huestis, and M. Saeed
Molecular Physics Laboratory, SRI International, Menlo Park, California 94025
(Received 2 March 1993)

Spatial distributions of photoelectrons produced by multiphoton ionization of xenon atoms are recorded by projecting the expanding photoelectron cloud onto a two-dimensional position sensitive detector. The projected image provides a direct view of the squared angular wave functions of the free electrons as well as their energy distribution. The results confirm recent observations that intermediate state resonances with $5f$ and $4f$ character establish the dominant ionization paths at low intensity, for short pulse excitation at 640 and 620 nm. At higher intensity more complex superpositions occur with formation of electrons with continuous distributions at low energies.

PACS numbers: 32.80.Rm

Photoelectrons generated at a point source with a discrete energy travel outward on the surface of a sphere that expands with time. For example, electrons produced at time $t=0$ with an energy of 1 eV can be found 20 ns later on the surface of a sphere of 25 mm diameter. This sphere can be projected onto a flat screen using an external electric field. A circular image results with a diameter that is proportional to square root the electron energy and a filling pattern that reveals the spatial distribution of the electrons on the surface of the sphere. In this way, the squared angular wave function of the free electrons is accessible to direct observation.

We have used this approach to investigate multiphoton ionization of xenon atoms in an intense laser field. Simultaneous visualization of the photoelectron energy and angular distributions facilitates the identification and classification of ionization mechanisms.

Recent work on multiphoton ionization of atoms and molecules by intense laser fields has shown that the dynamics of ionization are governed by the modification of the electronic structure of the target by the radiation field [1–7]. The effective energies of the electronic states are shifted (ac Stark effect) so strongly that the laser, which at low intensity was not resonant with any particular multiphoton transition, becomes resonant with individual intermediate states at specific critical intensities. One result is that the photoelectron energy and angular distributions often reflect the nature of the dominant intermediate states.

Consistent with previous experiments, we observe that at moderate intensities the photoelectron energies are discrete, appearing as if they had come from photoionization of the intermediate states, $E=h\nu-\mathrm{IP}(\text{intermediate})$, rather than from the ground state, $E=nh\nu-\mathrm{IP}(\text{ground state})$. This apparent nonconservation of energy results from the fact that photoelectrons do not recover the ponderomotive energy under conditions such that the product of the laser pulse duration and the electron velocity is much smaller than the spatial dimensions of the laser focus [1,2]. Our photoelectron angular distributions show that predominantly the $m=0$ component of the intermediate state is being ionized. This is likely a result of the larger $m=0$ to $m=0$ matrix elements in multiphoton transitions. At higher laser intensity the photoelectron energies broaden, and new features arise that are difficult to assign to specific intermediate states, pointing to additional ionization mechanisms.

A schematic of our experimental setup is shown in Fig. 1. A homogeneous acceleration field (typically 80 V/cm) is established by a pair of grids spaced 10 cm apart and cylindrical guard rings of 10 cm inner diameter. The laser beam is focused by a 15 cm lens to the center of the acceleration region. Helmholtz coils mounted outside the vacuum chamber (base pressure 4×10^{-10} Torr) reduce the Earth's magnetic field in the interaction region to below 10 mG. A pair of 2 in. diam microchannel plates are positioned behind the grid to which electrons passing the grid are extracted. Electrons exiting the channel plates are accelerated to 7 keV to impact on an ultrahigh vacuum grade phosphor screen. The screen phosphorescence is accumulated on the charge-coupled-device elements of a commercial video camera for typically 10 ms following the laser shot. The laser energy is measured for each shot and used to select images that fall in a prescribed energy range. The camera analog output is digitized (8 bit) and summed in computer memory in an

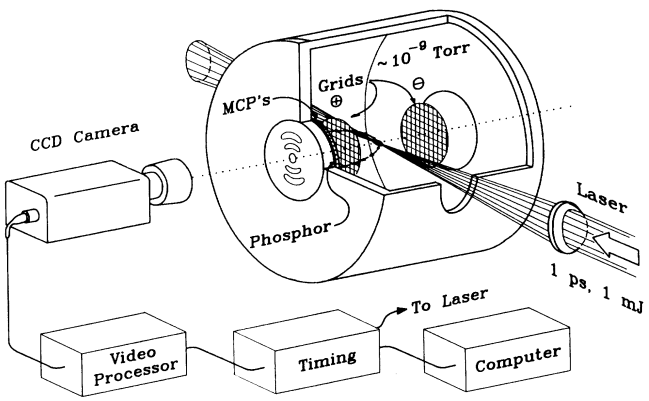

FIG. 1. Schematic of photoelectron imaging spectrometer.

array with pixel pattern of 256 by 240 with 21-bit intensity resolution. The effective frame capture rate is about 5 Hz.

Inspection of the equations of motion shows that when the ratio of electron energy, W, to the energy gained in the dc acceleration field, U, is kept small, the impact positions resulting from projection by the dc field very closely resemble the idealized projection in which electrons first expand for a fixed time and are then frozen in space and projected onto the detector plate. For example, when a field of 80 V/cm is used over an acceleration distance of $L=5$ cm the impact positions are equal to the idealized projection to better than 200 μm for electron energies of 1 eV and to better than 400 μm for electrons of 4 eV energy. The maximum deviations occur for electrons emitted near an angle of 45° toward and away from the detector plane. These deviations from the idealized projection should be compared with the overall size (D) of the projected images for the above-mentioned conditions: $D=4L(W/U)^{1/2}$. For instance, for 1 eV energy the electrons fall within a circle of diameter 1 cm; for 4 eV energy within a circle of 2 cm diameter.

In our experiments the drift chamber is filled with xenon to pressures of typically 10^{-8}–10^{-6} Torr. At these pressures approximately 50–5000 atoms lie within the focal volume of the laser beam (as defined by $1/e^2$ peak intensity). All images shown in this paper are accumulated from typically 2×10^4 laser shots each (about 1 h of summation at 10 to 100 electrons/shot). The images shown below represent the raw data without background subtraction or smoothing. The absolute gray scale is given along with each image. The images are reproduced on a 2400 dots per in. printer with 8-bit gray resolution.

In Fig. 2 we show an example of an image obtained with a laser intensity of 1×10^{13} W/cm^2 at 640 nm and a laser pulse length of 1.5 ps. This image results from ionization of atomic xenon via the ac-Stark-shifted $4f$ intermediate state [1–4]. The laser polarization is parallel to the screen, along the vertical axis. The innermost circular portion of the image represents photoelectrons formed in 6+1 photon ionization via the $4f$ state. The electron energy associated with this image diameter is 1.08 eV. The image very clearly reveals four planes of minimum intensity that lie perpendicular to the laser polarization (and the figure). These minima indicate that a dominant contribution to this photoelectron spectrum arises from $l=4$ (g), $m=0$ electrons, aligned with the laser polarization as the quantization axis. Such a distribution is expected in one photon ionization of a resonant intermediate with aligned f character because of the propensity in excitation of $\Delta l=+1$ states. At larger separations from the center of the figure additional structured rings appear that are due to above-threshold ionization (ATI), corresponding to two-, three-, and four-photon absorption from $4f$. The electron energy associated with the outer ring structures is separated by the photon energy, in agreement with this identification. Since the angular momentum changes by 1 for each absorption step, a minimum in intensity at the equator is expected for the first ATI image as is indeed observed.

We have investigated the sensitivity of these images to the strength of the dc electric field used to project the electrons to the screen. Images obtained for field strengths in the range from 20 to 150 V/cm were compared explicitly. Except for the expected change in absolute size of the features, no change in relative contributions from the individual patterns, and no change in the angular distributions was noted. Hence, the dc Stark effect due to the projection field should not play a significant role in the multiphoton ionization processes studied here.

For a linearly polarized laser we expect that the elec-

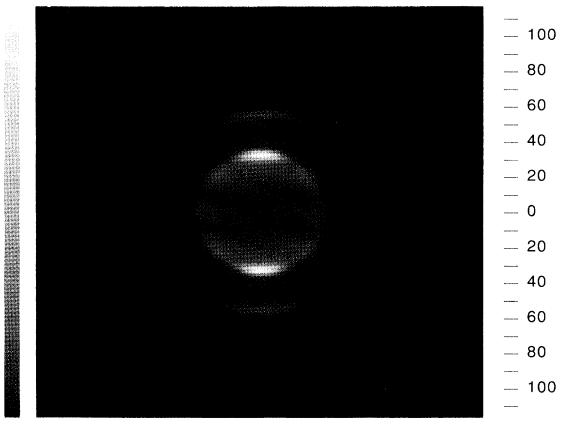

FIG. 2. Photoelectron image of xenon at 640 nm at 1×10^{13} W/cm^2. The image from one-photon ionization of the ac-Stark-shifted Xe($4f$) state occupies the central part of the figure (rows -35 to $+35$). Rings at rows ±55, ±72, and ±85 are due to above-threshold ionization of the $4f$ state. The laser polarization is along the vertical axis.

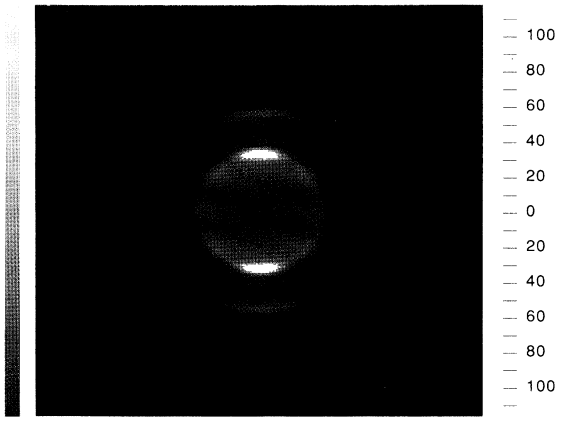

FIG. 3. As in Fig. 2, but laser polarization is perpendicular to the frame.

tron emission pattern is cylindrically symmetric around the laser polarization. This can be tested by switching the laser polarization to point toward the detector screen. Figure 3 shows that indeed a symmetric electron pattern appears. The cylindrical symmetry allows us to deconvolve the image in Fig. 2 using an Abel inversion, to obtain the original surface density on the constant-energy sphere. Figure 4 gives angular distributions derived from the images in Figs. 2 and 3 as obtained from an Abel inversion.

In Fig. 5 we show images obtained at a wavelength of 620 nm at three different peak laser intensities. Figure 5 shows two general features: (1) a bright central ring (from $4f$ and $5f$ intermediates) and corresponding outer ATI rings and (2) development of complex structures inside the central ring.

At the lowest intensity, 1.5×10^{13} W/cm^2, Fig. 5(a) shows that the dominant ionization channel is via the Xe($5f$) state resulting in a characteristic angular distribution of the outgoing electron with dominantly $l=4$ character. These electrons appear at an experimental energy of 1.47 eV. Inside the pattern arising from the $5f$ state a fainter image corresponding to contributions from the $4f$ state (at an energy of 1.18 eV) appears with a similar nodal pattern. Upon raising the intensity at 620 nm to 3.0×10^{13} W/cm^2 [Fig. 5(b)] contributions due to the $5f$ state weaken significantly in favor of the $4f$ state. At an intensity of 1×10^{14} W/cm^2 [Fig. 5(c)] the $5f$ contribution is no longer apparent [3].

Figure 5(a) shows weaker lower energy structures at about 0.25 and 0.06 eV. It is tempting to assign these to ionization via the $8p$ and $9p$ states to the $Xe^+(^2P_{1/2})$ ion-core state. Since the $8p$ and $9p$ states are of predominantly $Xe^+(^2P_{3/2})$ character we would expect to see much stronger contributions at the energies of 1.56 and 1.37 eV, corresponding to ionization into the $\frac{3}{2}$ core

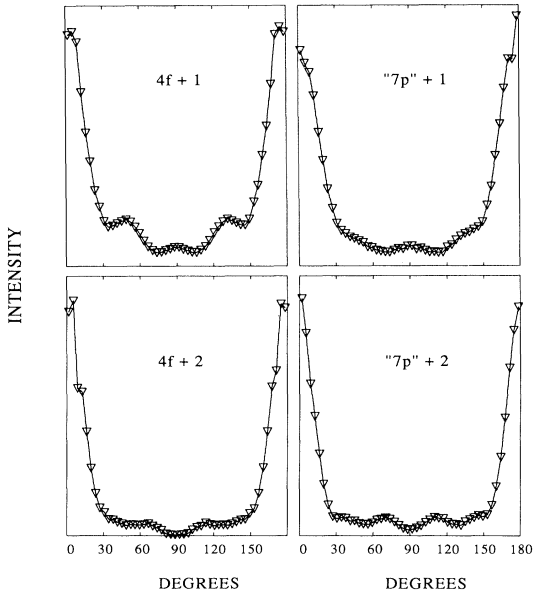

FIG. 4. Angular distributions obtained by Abel inversion for one- and two-photon ionization of the $4f$ and "$7p$" states.

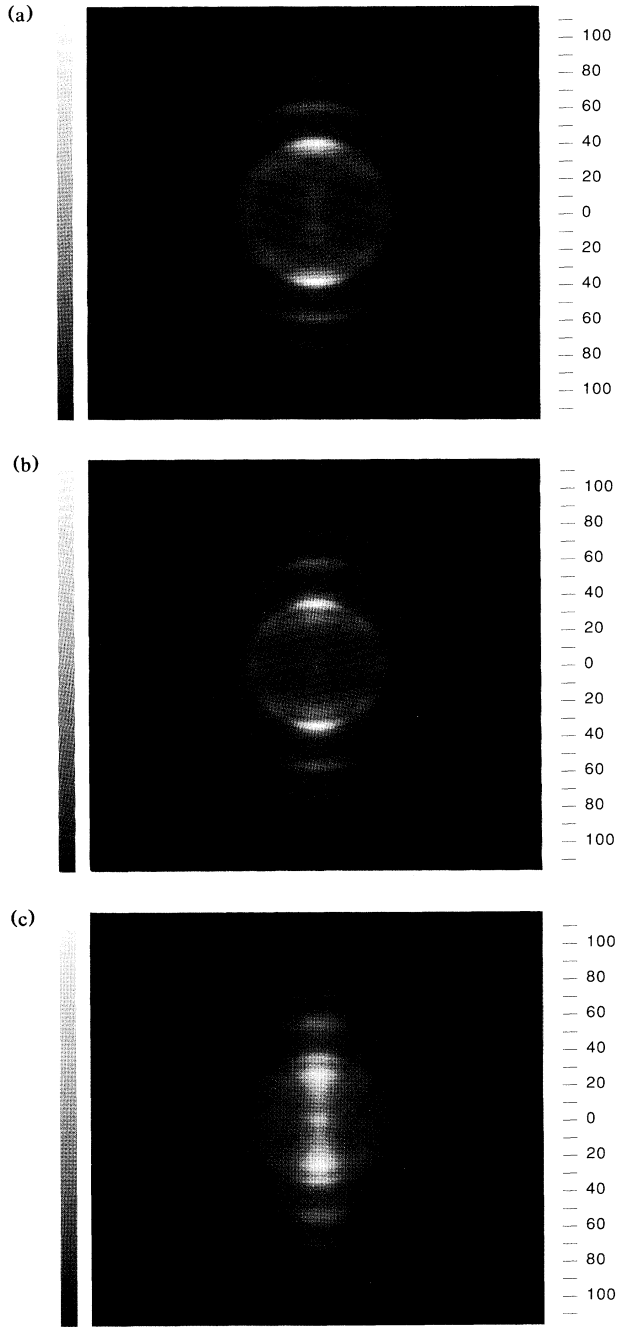

FIG. 5. Photoelectron images of xenon at 620 nm at various intensities. The laser polarization is along the vertical axis. (a) 1.5×10^{13} W/cm^2, row 40: $5f$ (brightest), row 36: $4f$, row 15:$9p$, row 11: $8p$. (b) 3×10^{13} W/cm^2, row 40: $5f$, row 36: $4f$ (brightest), row 28: "$7p$". (c) 1×10^{14} W/cm^2, row 36: $4f$, row 28: "$7p$" (brightest).

channel. We cannot identify these contributions with certainty since they overlap with the strong features that arise from the $5f$ channel. A further difficulty in assignment results from the fact that the angular distributions of the 0.26 and 0.06 eV features are much more concentrated along the direction of laser polarization than can be explained by simple angular momentum arguments.

At higher intensity [Figs. 5(b) and 5(c)] the low energy contributions disappear, because they are shifted out of resonance too early in the pulse, as is the $5f$ state [3]. They are replaced by a new contribution to the electron energy spectrum, appearing in Fig. 5(b) at an energy of 0.70 eV. This energy is somewhat lower than the energy expected from $6+1$ photon ionization of the $7p$ state if it were to shift in a purely ponderomotive way (then it should be observed at 0.85 eV). A peculiar property of this photoelectron peak is that its energy distribution extends to ever lower values as the intensity is raised, while the position of maximum intensity stays fixed [see Fig. 5(c)]. The angular distribution is also unexpectedly concentrated along the laser polarization (see Fig. 4). Similar observations were made at 640 nm (not shown). The quasicontinuous and misplaced "$7p$" feature has also been observed in previous investigations [3,7] but its angular distribution has not been studied.

The energy resolution of our device actually improves with decreasing electron energy, so we can assert that the observed widths reflect that these electrons arise from a more complex ionization mechanism. One possibility is that the unidentified intermediate states(s) are subject to ac Stark shifts that are nonlinear in the laser intensity or do not shift by the same amount as the continuum. Such an effect might occur through near resonance between the laser frequency and the $7p$-$7d'$ transition. A second possibility is that several intermediate states are contributing simultaneously. For example, the $7d'$, $6s'$, and $6d'$ states will be shifted into seven-photon resonance at higher intensities. These states can contribute to the photoelectron spectrum as a consequence of autoionization into the $(\frac{3}{2})$ channel giving rise to electrons at 0.696, 0.447, and 0.328 eV, respectively. The energy resolution of our apparatus should suffice to resolve discrete contributions at these energies.

Finally, as motivated by the narrow angular distributions for low energy electrons and their continuous energy distribution, we suggest that the appearance of these electrons requires a modification of the generally accepted mechanism of ionization via ac-Stark-shifted resonances [1–4,7] in that an ionization mechanism must also be active that can lead to a continuous distribution of low energy electrons. The possibilities for such a channel are (a) a growing contribution from nonresonant ionization, (b) tunneling ionization due to the periodic lowering of the Coulomb barrier by the intense laser field [7], or (c) double ionization. We are encouraged that an additional mechanism is required because unpublished work in our laboratory on He and H_2 indicates that continuous, low energy, and narrow angle distributions are a general phenomenon in intense field laser ionization. These contributions are suppressed in conventional photoelectron spectrometers because of their inherent insensitivity to very low energy electrons. Our technique gathers simultaneously all of the information that can be obtained by conventional techniques. Actually seeing the energy and angular distributions, for even very low energy electrons, helps in the assignment of specific ionization paths and should provide a useful tool for characterizing photoionization processes.

This experiment was made possible by the National Science Foundation under Grant No. PHY-9249199.

[1] R. R. Freeman, P. H. Bucksbaum, H. Milchberg, S. Darack, D. Schumacher, and M. E. Geusic, Phys. Rev. Lett. **59**, 1092 (1987).

[2] T. J. McIlrath, R. R. Freeman, W. E. Cooke, and L. D. van Woerkom, Phys. Rev. A **40**, 2770 (1989).

[3] P. Agostini, P. Breger, A. L'Huillier, H. G. Muller, G. Petite, A. Antonetti, and A. Migus, Phys. Rev. Lett. **63**, 2208 (1989).

[4] H. Rottke, B. Wolff, M. Tapernon, K. G. Welge, and D. Feldman, Z. Phys. D **15**, 133 (1990).

[5] S. Allendorf and A. Szöke, Phys. Rev. A **44**, 518 (1991).

[6] H. Helm, M. J. Dyer, and H. Bissantz, Phys. Rev. Lett. **67**, 1234 (1991).

[7] E. Mevel, P. Breger, R. Trainham, G. Petite, P. Agostini, A. Migus, J.-P. Chambaret, and A. Antonetti, Phys. Rev. Lett. **70**, 406 (1993).

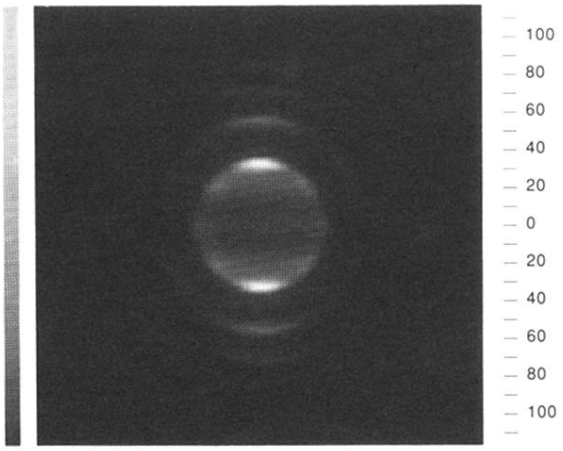

FIG. 2. Photoelectron image of xenon at 640 nm at 1×10^{13} W/cm^2. The image from one-photon ionization of the ac-Stark-shifted Xe($4f$) state occupies the central part of the figure (rows -35 to $+35$). Rings at rows ±55, ±72, and ±85 are due to above-threshold ionization of the $4f$ state. The laser polarization is along the vertical axis.

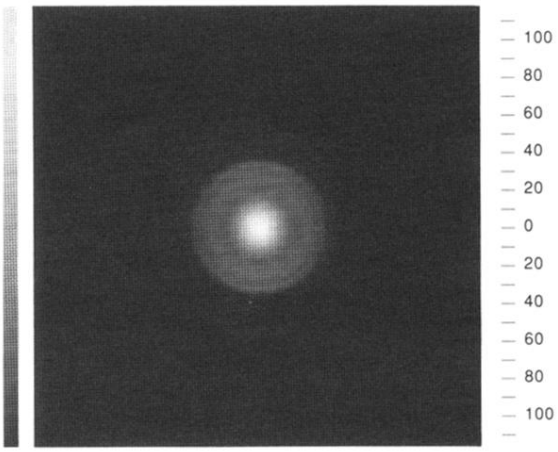

FIG. 3. As in Fig. 2, but laser polarization is perpendicular to the frame.

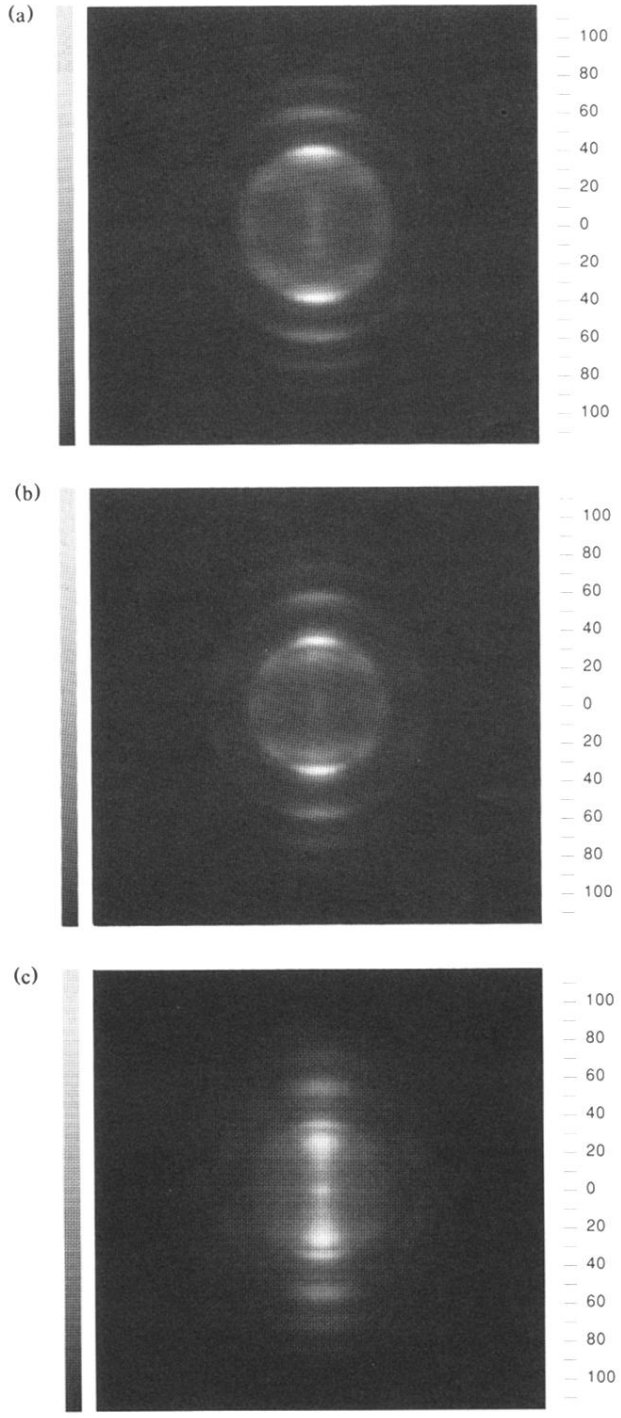

FIG. 5. Photoelectron images of xenon at 620 nm at various intensities. The laser polarization is along the vertical axis. (a) 1.5×10^{13} W/cm^2, row 40: 5*f* (brightest), row 36: 4*f*, row 15:9*p*, row 11: 8*p*. (b) 3×10^{13} W/cm^2, row 40: 5*f*, row 36: 4*f* (brightest), row 28: "7*p*". (c) 1×10^{14} W/cm^2, row 36: 4*f*, row 28: "7*p*" (brightest).